Effects of inert fuel diluents on the dynamic state of a thermoacoustically unstable gas turbine combustor

E. Karlis* ,Y. Hardalupas † and AMKP Taylor ‡
Imperial College London, London, SW7 2AZ, UK

The effects of inert diluents in the fuel mixture of a model swirl stabilized gas turbine combustor, under thermoacoustically unstable limit cycle operation, were studied experimentally. The measurements included Particle Image Velocimetry (PIV), high speed CH^* chemiluminescent imaging and dynamic pressure signals. The paper focuses on the dynamic phenomenon of the period doubling bifurcation, which came about when the equivalence ratio (ϕ) of undiluted flames was enriched from 0.55 to 0.60 under constant Reynolds number (Re). The bifurcation featured an emergence of an aerodynamically related timescale in addition to the fundamental timescale which was induced from an unstable acoustic eigenmode. The aerodynamic timescale is introduced by azimuthal convection of a high heat release rate region, and is linked in the literature with a precessing motion of the recirculation zone. Prior to the bifurcation, the flame anchored between the wall and the outer shear layers of the recirculation zone assuming a V-shape. The dynamics were attracted to a Period-1 limit cycle. Post the bifurcation the flame expanded in the inner shear layers of the recirculation zone assuming an M-shape, while the dynamics were attracted to a Period-2 limit cycle. The latter operational condition was subject to nitrogen dilution in order to parametrically increase the molar fraction of inert diluent in the fuel stream. It was found that on increasing the diluent molar fraction the amplitude and the frequency of the limit cycle fundamental acoustic mode decreased. Also, inert dilution suppressed the aerodynamic timescale and the flame assumed a V-shape again. A mechanism to interpret this mechanism is suggested. Increasing the diluent molar fraction of the fuel makes the flame susceptible to quenching because the extinction strain rate of the mixture decreased. Thus, the flow imposed strain rates quenched the flame when it attempted to anchor on the inner shear layers of the vortex breakdown induced recirculation zone. The inability of the flame to anchor on the shear layers suppressed the aerodynamic mode. The paper argues that the existence of inert diluents in the fuel can significantly alter the dynamic state of the combustor, since the anchoring locations of the flame greatly depend on the composition-sensitive extinction strain rate of the mixture.

I. Introduction

The gas turbine combustor design process entails multiple considerations that importantly include the emission performance in respect with the regulatory restrictions and requirements. A key driver of gas turbine research is the development of technically premixed swirl stabilized combustors that operate in the lean regime to reduce the thermal NO_x emissions [1]. An additional design consideration is introduced by the variability of the fuel used for land based power production. Ideally the burner should be able to accommodate combustion of variable composition as the latter is largely varying between different sites of fuel production, or on a day to day basis from the same site [2]. An inherent issue of the lean premixed mode of operation is the demonstration of combustion instabilities [3], wherein the acoustic and thermal fields of the combustor couple in a self amplifying manner, until a thermoacoustically unstable limit cycle regime is established [4]. The regime may cause cyclic dynamic pressure loading that can lead to component failure. The fuel composition may well affect the dynamic regime of the combustor, since the flame anchoring locations are substantially affected by the fuel mixture properties, modifying the phase difference and leading to increased coupling between the thermal and acoustic signals and triggering thermoacoustic instabilities. A widely

*PhD Candidate, Mechanical Engineering, SW7 2AZ, UK, e.karlis15@imperial.ac.uk
†Professor, Mechanical Engineering, SW7 2AZ, UK, y.hardalupas@imperial.ac.uk
‡Professor, Mechanical Engineering, SW7 2AZ, UK, a.m.taylor@imperial.ac.uk

used fuel interchangeability index is the fuel Lower Wobbe Index (LWI). It is defined as:

$$LWI = \frac{LHV}{\sqrt{SG}} \tag{1}$$

where LHV is the fuel lower heating value and SG is the specific gravity. Given identical fuel line pressure and pressure drop between two fuels, the heat release rate will be equal between the two fuels if they are characterized by similar LWI values [5]. Nevertheless the LWI does not incorporate information regarding the fuel composition and the effective burning rate, adiabatic flame temperature or resistance to extinction, even though such properties dictate significantly the dynamic behaviour of the engine. The authors in [6] underlined that fuel composition may affect the combustor stability boundaries. They recognized the significance of a premixture characteristic transport time, which is a summation of advection and reaction timescales. Fuel composition could adjust these timescales and the stability map of the combustion operation. In [7] the authors reported that the behaviour of fuel constituents comprising a mixture may differ significantly than the resulting mixture due to altered transport properties and burning speeds. They investigated the effect of increasing levels of turbulence on the nonlinear combustion behaviour of fuels with varying composition. Mixtures with similar laminar flame speeds demonstrated substantial variation on the turbulent consumption velocities, hence the effective operational behaviour of the combustor was dependent on the relative molar fraction of each constituent. In [8], the authors identified thermoacoustic stability indicators based on the pathway of the centroid of the heat release rate on adjusting operational conditions and fuel properties. It was showed that flames with similar shapes would demonstrate similar dynamic behaviour. They concluded that since the heat release centroid was affected by the fuel composition and given that the centroid location distinguished explicitly between unstable and stable operational conditions the transport time delay of the premixture to the centroid determined the stability boundaries. In [9] the authors reported that the addition of inert diluents in the mixture secured constant flame temperatures but at the same time resulted in adjustment in the characteristic convective time delays and a reduction in the limit cycle amplitudes in both the high and low swirl burner configurations they examined.

The above observations motivate the current study. Focus is brought on the fuel composition variability, particularly on inert fuel diluents and their effect on the thermoacoustic dynamics. The combustor demonstrated a particular dynamic behaviour, namely the period doubling bifurcation from a Period-1 limit cycle to a Period-2 limit cycle. In the latter, aerodynamic timescales were superimposed on the acoustic timescales which dictated the fundamental frequency of a limit cycle. The effects of inert diluents in the fuel were shown to drive the combustor to either the Period-1 or Period-2 limit cycle, even though the LWI of the mixtures did not differ more than 10% between the limit cases that were examined. The two dynamic states featured anchoring on different flow topologies. It was thereby concluded, that minute changes in fuel composition may lead to different dynamic regimes and flame shapes, hence an additional dictating parameter needs to be considered. Since literature consensus is that the flame anchoring locations play a substantial role in the establishment of thermoacoustic instabilities on varying fuel composition, the extinction strain rate was considered as an additional scaling parameter of the instabilities. It was shown in [10] and in [11] that the flame assumed different configurations provided that it was able to sustain increased strain from the local flow topology. Resistance to flow imposed straining was quantified via the mixture extinction strain rate. This concept is introduced in the current work, to interpret flame shape and dynamic behaviour transitions between Period-1 and Period-2 limit cycles. The rest of the paper is structured as follows: Section II describes the experimental configuration and identifies the operational cases; section III presents the manifestation of the period doubling bifurcation for an undiluted flame on increasing the equivalence ratio on a constant Reynolds number; section IV deals with the effects of nitrogen dilution, while the combustor experienced Period-2 oscillations, section V describes the mechanism of the Period-2 suppression on increasing diluent molar fraction and finally section VI summarizes the results and conclusions of the current research work.

II. Experimental Configuration

An overview of the experimental configuration that is employed in the current study is provided in Fig. 1 and in Fig. 2. The configuration was similar to previous works [12–14]. Compressed air was provided at 4 barg, measured through a thermal mass flow meter (M+W Instruments, Mass Stream D-6280) and controlled through a thermal mass flow controller (M+W Instruments, Mass Stream D-6383). The air flow was regulated through the following equipment. A pressure reducer was installed (Backpressure Regulator, Mackenberg UV 5.1) upstream of a critical Venturi (Cussons Technology Ltd, BS/ISO 9300:2005). The critical Venturi nozzle was used to choke the flow and provide a sonic

boundary. The flow profile was conditioned before the nozzle through a tube bundle containing a wire mesh gauge and a flow straightener. Upstream and downstream of the Venturi nozzle two absolute pressure gauges were installed (Omega, PXM319-3.5A10V) to estimate the extent of chocking across the nozzle. An additional microphone was mounted in the premixing duct upstream the swirler and downstream the sonic nozzle to pursue pressure measurements which were translated into velocity fluctuations of a standing wave via the two-microphone method [15].

Two thermal mass flow meters (M+W Instruments, Mass Stream D-6250, measurement uncertainty± 0.625 g/s, 3% factory accuracy at full scale) measured the mass flow rate of the fuel and the diluent. The mass flow streams comprising the fuel supply were controlled through two thermal mass flow controllers (M+W Instruments, Mass Stream, D-6320, measurement uncertainty ± 0.01 g/s, 1% factory accuracy at full scale). The two streams were combined directly downstream the fuel controllers and a pipe length of $4m$ secured homogeneous mixing. The fuel mixture entered the injector at the rear of the centerbody and was forced out of ten equally spaced holes in the swirling annular air flow. Another absolute pressure gauge (Omega, PXM319-3.5A10V) measured the pressure in the fuel delivery line to secure that in each experimental case fuel supply was uncoupled from the dynamics in the combustor. In Fig. 2 the air flows from left to right. The majority of the air (90%) was delivered to the swirler, while a smaller amount flowed through the centerbody for cooling purposes. The swirler technically premixed the reactants with the oxidizer in a similar manner to industrial gas turbine combustors [16]. The resulting swirl number is approximately 0.7, based on the formulation suggested in [17].

A. Signal Acquisition

Downstream the swirler, the air-fuel mixture is expanded through a diffuser. The premixture was introduced into a 1.2 m long tube combustor. A cylindrical fused quartz with 70 mm internal diameter and 2 mm wall thickness allowed 360^o optical access to the flame. The quartz tube length was 450 mm. At the end of the quartz tube section, a tapping allowed a spark plug igniter to access the ignitable mixture. A tapping 50 mm downstream of the igniter accommodated the installation of a semi-infinite tube (SIT) configuration. It consists of a coiled seamless tube of 2.93 mm internal diameter, whose length was 2 m to avoid any interference with the acoustic field. It was connected to a plastic hose for nitrogen flow for cooling purposes of the installed dynamic microphone (Kulite MIC-190M, nominal sensitivity: 0.0035mV/Pa at 160 dBa excitation). The microphone was installed 130 mm over the bore of the exhaust and acoustic waves from the combustor were measured through a 1 mm hole drilled on the SIT configuration.

Chemiluminescence signals were acquired using a photomultiplier system developed by Panoutsos et al. [14]. Global chemiluminescent emissions from the transparent part of the combustor were detected by a set of UV plano-concave (Thorlabs, focal length -30 mm, diameter 1 in) and UV plano-convex (Thorlabs, focal length 35mm, diameter 1 in) lenses, focusing the light on a 1.3 mm diameter lens of an optical fibre (Thorlabs-FT1500UMT-0.39 NA, 300-1200 nm). The spectroscopic unit acquired the light transmitted through the optical fibre. The light was split into three spectral fractions using two dichroic mirrors. The reflected light was directed onto filters, to acquire the light from the spectra of interest (308.5 nm for OH*-bandwidth 1.8 nm, 430.5 nm for CH*-bandwidth 1.9 nm, 516.0 nm for C_2^* – bandwidth 10 nm). The pressure and chemiluminescence analogue signals were acquired and stored though a National Instruments data acquisition card. Data from the acquisition card in each experimental case were collected for 10 seconds at a sampling rate of 32768 Hz at segments of 1024 samples.

B. High Speed Chemiluminescent Images

For each experimental case, 5000 high speed CH^* images of the flame were captured at each experimental case at 3000 frames per second. The CH^* spatial distribution was selected as a surrogate of the spatial distribution of the heat release rate. In [18], it was shown experimentally in a premixed counterflow burner configuration, that increasingly strained methane flames preserve a linear relationship between the CH^* intensity and heat release rate. The camera (Photron HSS6-CMOS HighSpeed Star2) was equipped with a Nikkon lense (f/4.5, focal length 105mm) fitted with a narrow bandpass interference filter (432 ± 5 nm). The quantum efficiency of the camera at the examined optical range was 30%. The triggering of the camera was synchronous to the dynamic pressure signal. The method adopted in the current campaign to consistently initiate the triggering was the permutation entropy, which has been described in a previous work [19]. A dip in the permutation entropy signal signifies that the combustor dynamics are attracted from an unstructured low amplitude mode to a high amplitude low complexity limit cycle. The transition from a high entropy signal, characteristic during quiescence, to a low entropy one, as is the case during limit cycle combustion was

essentially the triggering indication. The camera acquisition lead the permutation entropy triggering signal by 300 images in order to capture events before the onset of an instability. The resolution of each image is 300 x 900 pixels, and the size was 70 mm by 210 mm hence each pixel resolves 0.056 mm^2 of the imaging area. The spatial location of the high speed CH^* imaging window is described in Fig. 2. High speed flame imaging measurements were carried out independently from the PIV measurements.

C. High Speed Particle Image Velocimetry

The time dependent structure of the flow field was through high speed Particle Image Velocimetry (PIV) experiments. Micron alumina particles were used to seed the flow, using a cyclone seeder. The illumination source was an Edgewave Nd: YAG laser double pulsed at a rate of 3 kHz, emitting light at 532 nm. Pulse energies were 4 mJ/pulse and their relative time distance between each pair of illuminations was equal to dt=4 μs. The laser beam was formed by employing the optical configuration presented in Fig. 3 to create a profile with an approximately 1 mm waist thickness. The Mie scattering signal was captured with a Photron CMOS HighSpeed Star 2 equipped with a Nikkon lense (f/4.5, focal length 105mm) at a resolution of 1024x992 pixels. The lens was fitted with a narrowband filter (Edmund Optics, 532 nm ± 5 nm) to suppress flame chemiluminescence from contaminating the image. Unavoidably, reflection lines along the longitudinal axis were captured, due to the cylindrical shape of the optical confinement. They were suppressed using a polariser. It successfully suppressed reflections and secured the CMOS of the camera was not saturated, in the expense of the signal to noise ratio of the alumina particles. The time stamp of each illumination pulse was explicitly defined by extracting the high intensity peaks in the photomultiplier C_2^* signal. This assisted in precisely extracting the coherent component of the flowfield oscillations.

The location of the axial-radial cross sectional plane downstream the outlet of the diffuser is denoted in Fig. 2. The sides of the combustor upon which the laser sheet was impinging were masked out of the post processed vector fields, as the polariser did not suppress those reflections adequately. The axial-radial cross section had an effective spatial resolution of 60 mm by 60 mm. Synchronisation between the illumination source and the camera acquisition was achieved through LaVision's Davis 7.2 software, while the post processing and vector extraction of the raw Mie scattering images was achieved through LaVision's 8.4 software. The size of the final interrogation window was 32 pixel by 32 pixel with 75% overlap. This post processing scheme resulted in vectors spaced over increments of 0.46 mm.

A representative mean flowfield is presented in Fig. 4. The flowfield is a result of 2800 images while the combustor showcased limit cycle thermoacoustic instabilities. The direction of the flow is from top to bottom. The uppermost boundary of the flowfield, i.e. the 0 mm axial section coincides with the end of the optically inaccessible diffuser. Streamlines are superimposed on velocity vectors. The red coloured vectors denote regions of negative axial velocity, whereas blue coloured vectors denote regions of positive axial velocity. The flowfield features a vortex breakdown-induced recirculation zone and a region of free stream velocity. The boundary between these topologies defines shear layers of zero axial velocity. The extent of the zero axial velocity contours are marked with a green dashed line. Shear layers provide adequate residence time scales for the flame to anchor upon. In contrast to same purpose experimental configurations the flowfield did not feature an outer recirculation zone, because the diffuser secures gradual expansion downstream the inlet of the swirler and not a sudden step expansion. The latter would cause flow separation and effectively an outer recirculation zone.

D. Operating Conditions

The experimental campaign pursued to increase understanding of the effects of inert diluents on the dynamic state of the combustor and the thermoacoustically unstable combustion of propane. For this purpose, two subsets of measurements were considered. In the first subset, the Reynolds number (Re=$\frac{UD}{\nu}$, where U is the bulk velocity, D is the combustor inner diameter, and ν in the viscosity at room temperature) was kept constant at 18000, while the equivalence ratio (ϕ) increased from 0.55 to 0.60. The second subset involved nitrogen dilution of the 0.60 equivalence ratio mixture. The dilution method involved maintaining the mass flow rate of propane constant and increasing the mass flow rate of nitrogen. Thus, the effective molar fraction of propane in the fuel decreased, while the diluent's molar fraction increased. The global equivalence ratio and Re were fixed at their nominal values via minute adjustments of the air flow rate. The characteristics of each experimental case are presented in Table 1, wherein the equivalence ratio, the characterization of the dynamic state, the molar fraction χ of inert diluent in the fuel, and the adiabatic flame temperature of the mixture are presented.

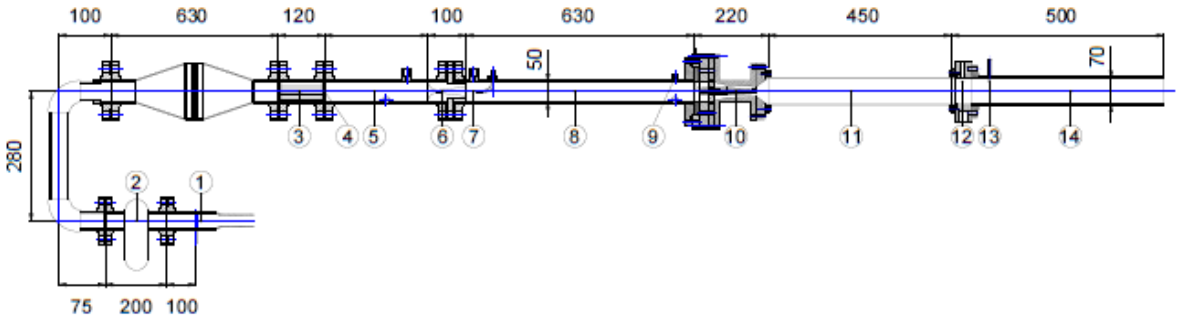


Fig. 1 Lean premixed model gas turbine combustor rig, [20]. Dimensions in mm. 1. Upstream fuel supply (not used in this campaign), 2: Air flow supply backpressure regulator, 3: Flow straightener, 4: Wire mesh gauge, 5: Flow pre conditioner, 6: Critical Venturi nozzle. 7: The two indicated ports were either used for seeding the flow with alumina particles, or for the upstream duct velocity measurements via the two microphone method 8: Sonic flow settling length, 9: Pressure tapping, 10: Swirler, 11: Fused silica window section, 12: Spark plug igniter, 13 Dynamic pressure microphone tube tapping, 14: Exhaust.

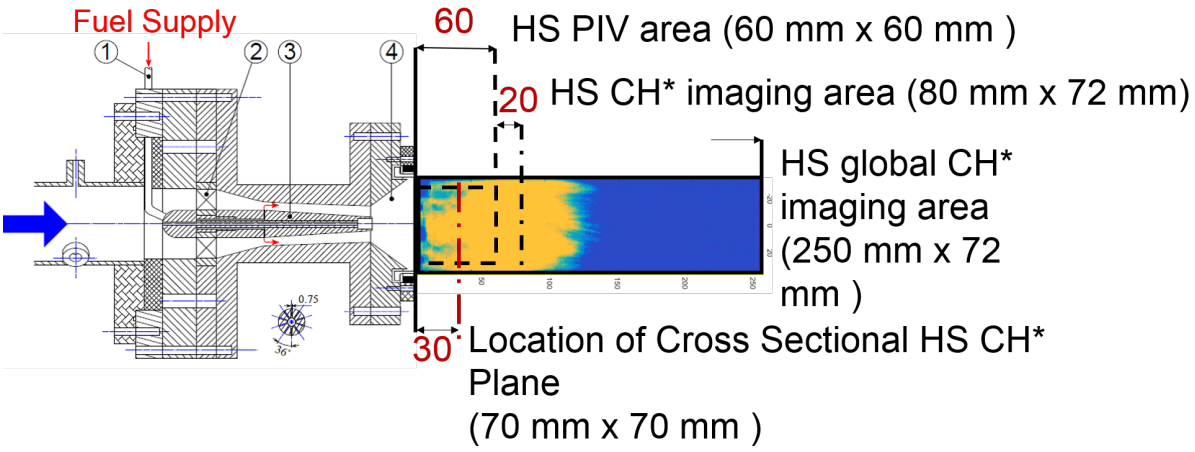


Fig. 2 The combustor geometry, with the dimensions of the high speed (HS) PIV and CH^* imaging planes in mm. 1: Fuel Supply Line, 2: Location of blades, 3: Centrebody, 4: optically non-accessible diffuser.

Figure 5 characterizes the operational conditions in terms of their regime on Peters [21] turbulent combustion diagram. The diagram concerns fully premixed flames, whereas the flame in the current campaign is technically premixed. The root mean square values of the turbulent intensity fluctuations (u') and the integral length scale (l) have been identified with the help of the PIV measurements. The unstretched laminar flame speed (S_L) and the flame thickness (δ_L) have been identified using the software Cantera [22] through the flame speed simulation module, using the GRI-MECH 3.0 [23] chemical kinetics and transportation mechanism. The flame thickness was calculated by the maximum temperature gradient across a normalized frame front profile, an approach given in [24]. All of the flames examined in the current paper belong to the thin reaction zone regime, wherein turbulent eddies can penetrate into the preheat zone but not into the reaction zone. The flame may be treated as a stretched laminar flame surface, with burning rate variations induced by turbulent stretching. These observations allow one to consider in the rest of the paper that the flame is locally behaving as a stretched laminar flamelet. Fundamental considerations are employed to reduce the response of the turbulent flame to the flow imposed strain rate disturbances, to mixture properties.

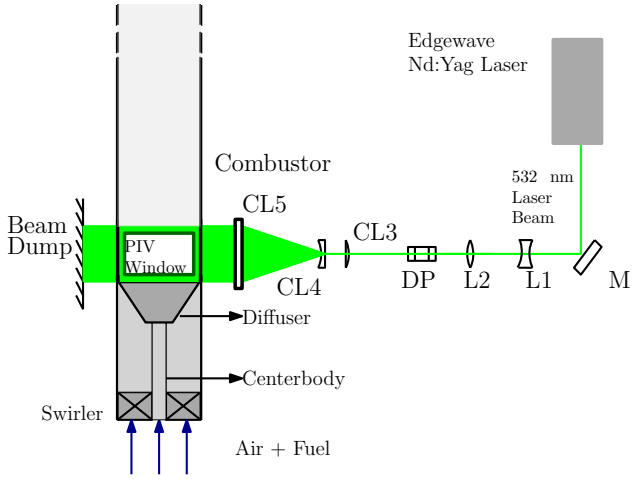


Fig. 3 A top view of the optical configuration employed to generate the light sheet for the axial-radial field of view of the high speed PIV measurements. The HSS6 camera is placed below the combustor perpendicularly to the direction of the laser beam (not shown here). M:Mirror, Lense L1: -100mm, L2: 150mm, DP: Dove Prism, Cylindrical Lense CL3=400mm, CL4=-40mm, CL5=1000mm.

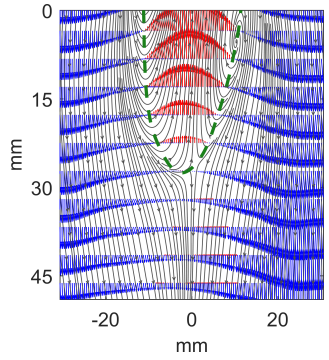


Fig. 4 Identified mean flowfield corresponding to Case 2 (see Table 1). Streamlines are superimposed on red and blue coloured vectors indicating negative and positive axial velocity. The green dashed line indicates the extent of the recirculation zone. Blue vectors form a free stream region and red vectors identify a vortex breakdown induced recirculation zone. An outer recirculation zone is not established in the current geometry, due to existence of the diffuser (see Fig. 2 and Fig. 3).

III. Period Doubling Bifurcation

The current section focuses on the period doubling bifurcation one observes on increasing the equivalence ratio under constant Reynolds number. Figures 6 and 7 show dynamic pressure and heat release rate indicative signals and spectra for Case 1, phi = 0.55 and Case 2, ϕ = 0.60 respectively. In both figures, the spectra of both signals feature a distinct peak at the fundamental frequency of instabilities f_f, equal to 160 Hz for case 1 and 175 Hz for case 2. These frequencies correspond to the first quarter wave mode of the duct, which are identified by considering a closed to open ended duct, with upstream closed end boundary condition, $u\prime$=0 and downstream open end boundary condition $p\prime$=0. The distinct feature between the two cases is the emergence of a subharmonic frequency f_h in the spectra of the richer condition equal to f_h=87 Hz. The emergence of a non harmonic to the fundamental frequency introduces an additional time scale dictating the oscillations of the combustor. This has a distinct effect in the dynamic characteristics of the limit cycle. Prior to the period doubling bifurcation the dynamics are attracted to a single loop locus of attraction, whereas post the period doubling bifurcation the dynamics are attracted to a double loop, higher amplitude attractor. The attractors of dynamic pressure signals are shown in Fig. 8. The reconstruction of the locus of attraction followed the method proposed by Takens [25] to approximate the actual system dynamics out of single scalar measurements. The method reconstructs the signal in the phase space by creating vectors out of the values of the scalar measurements.

Table 1 Identification of the examined cases. The Reynolds number was Re=18000. The fuel was bottled propane whose molar fraction in the fuel was reduced through nitrogen dilution. In the table we present the equivalence ratio, the dynamic state of the combustor, the molar fraction χ of the N_2 diluent and the adiabatic temperature T_{ad} that characterizes each fuel.

Case ID	ϕ	Dynamic State	χ:N_2	T_{ad} [K]
1	0.55	Limit Cycle, Period 1	0	1611
2	0.60	Limit Cycle, Period 2	0	1720
3	0.60	Limit Cycle, Period 2	10	1702
4	0.60	Limit Cycle, Period 2	20	1688
5	0.60	Limit Cycle, Period 2	30	1681
6	0.60	Limit Cycle, Period 1	40	1675
7	0.60	Limit Cycle, Period 1	50	1669

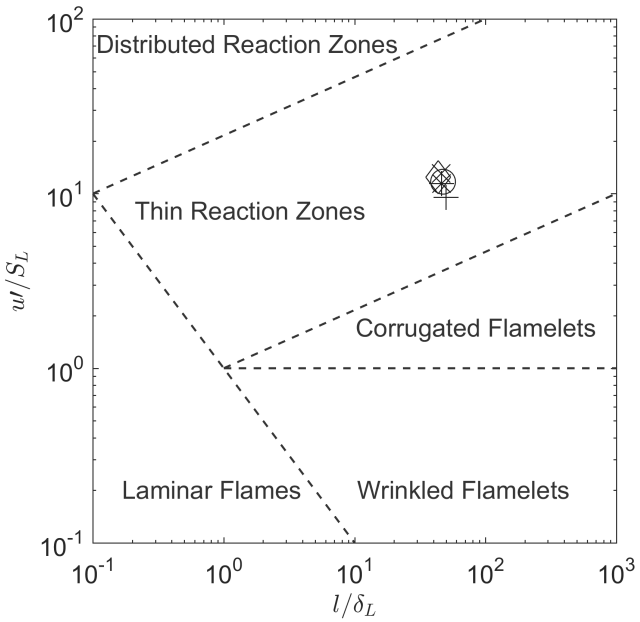


Fig. 5 Estimation of the flamelet regime on the turbulent premixed combustion diagram by Peters [21]. Case 2: $\diamond$, Case 3: $\times$, Case 4: $*$, Case 5: $\bigcirc$, Case 7: + .

Successive elements of the vector are samples whose time distance τ is equal to the first crossing of the autocorrelation function of the signal with the abscissa axis, which grants statistical independence of successive vector dimensions.

The reason for the emergence of the subharmonic instability is not related to coupling with an unstable acoustic eigenmode of the combustor at this frequency. This is confirmed by developing a linear acoustic model, similar to the one in [26] to identify all the potential unstable eigenmodes of the geometry for the given operational conditions. The model accounts for the relationship between incident acoustic perturbations and unsteady heat release rate by embedding the n-τ model [27]. The parameter τ corresponds to an axial convective time delay from the point of introduction of reactants in the combustion chamber up to the centre of gravity of the flame. It effectively dictates the phase difference θ between the heat release rate and the incoming velocity fluctuations. The parameter n is the gain of the transfer function between the incoming velocity petrubations and the effective heat release rate at the fundamental frequency of instabilities. Figure 9 shows the results of the model as a function of θ with n provided as a parameter to

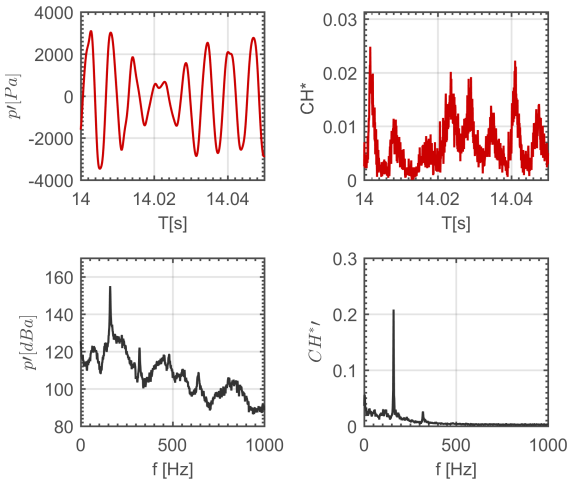


Fig. 6 Left Column: Dynamic pressure signal (top) and Fast Fourier Transformation Spectra (bottom) of Period 1, ϕ=0.55 limit cycle oscillations. Right Column: CH* global intensity (top) acting as a proxy of heat release rate and Fast Fourier Transformation Spectra (bottom).

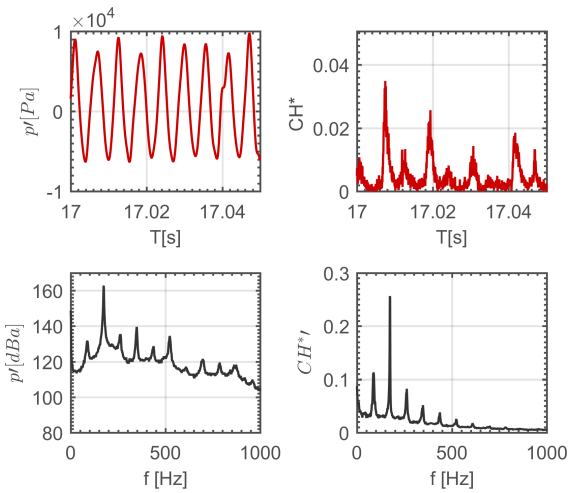


Fig. 7 Left Column: Dynamic pressure signal (top) and Fast Fourier Transformation Spectra (bottom) of Period 2, ϕ=0.60 limit cycle oscillations. Right Column: CH* global intensity (top) acting as a proxy of heat release rate and Fast Fourier Transformation Spectra (bottom).

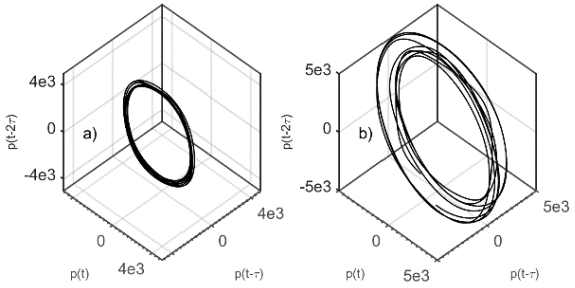


Fig. 8 Period-1 (left) and Period-2 (right) limit cycle attractors. The dynamic pressure locus of attraction are calculated according to the method developed in [25]. The time delay between the vector components of each point in the three dimensional down-projection of the dynamics is τ =0.0017.

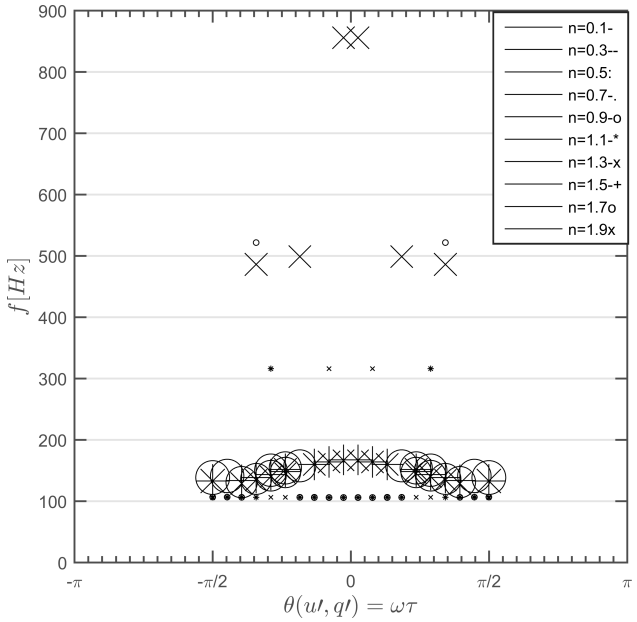


Fig. 9 Theoretically calculated unstable eigenfrequencies as a function of the phase difference between dynamic pressure and heat release rate. Big markers indicate positive growth rates. The parameter n is the gain defined as $n = \frac{Q\prime(\omega)}{u\prime(\omega)}$. The range of n values introduced to account for the dilatation rate of the flow mixture due to reaction has been identified experimentally. The speed of sound is a function of the adiabatic flame temperature of air-propane combustion with ϕ=0.60.

the calculations. The range of potential n values has been identified experimentally and is an input to the model. The adiabatic temperature of combustion of propane for ϕ=0.60 is used to calculate the speed of sound in the combustor. The marker size is linearly increasing on increasing growth rate values for each n, hence larger symbols indicate regions of unstable modes. One observes that in accordance to the experimental results, the unstable eigenmode is identified at a region of frequencies between 150 Hz and 178 Hz. On converging phase difference to 0 radians the coupling frequency increases, even though the adiabatic temperature is constant. The third and fifth quarter waves are deemed unstable for a single n value, even though such a transition to the dictating frequency of the dynamics has not been observed experimentally. Interestingly, the subharmonic region is not deemed unstable by the model, even though it correctly captures the fundamental eigenmodes. It is thereby concluded that the emergence of the subharmonic is related to a flow and flame interaction at this frequency, due to an aerodynamic phenomenon inherent to swirl stabilized flow fields.

The subharmonic frequency identified in same purpose experimental configurations, [29–32] has been attributed to coupling between the flame and a naturally excited global and absolute instability coherent structure namely the Precessing Vortex Core (PVC) [33–35]. The triggering mechanism is summarized as follows: axially propagating acoustic waves impinging on the swirler may produce axial and azimuthal instabilities, due to the interaction with the axially diverging swirling blades. Axial and azimuthal disturbances propagate downstream inside the combustor at the acoustic and the bulk velocity respectively [36]. On increasing amplitude of azimuthal disturbances the swirl number increases as well. The authors in [34] showed via linear stability analysis of a swirling flowfield whose azimuthal-radial section was modelled as a Rankine vortex, that on increasing swirl number, the rotational symmetry of an axially propagating disturbance on the vortex breakdown induced-shear layers structure loses rotational symmetry. On low swirl number the pertrubation propagates as a zero wavenumber Kelvin-Helmholtz instability, whereas on increasing swirl number the most dominant unstable wavenumber is equal to -1, namely, a helical wave develops counter-rotating to the direction of azimuthal rotation of the swirling flowfield. The development of the helical wave introduces a precessing motion of the recirculation zone, thereby modulating the flame surface, by advecting it off the axial axis of symmetry. It was showed in [29], that the PVC introduces a flame asymmetry that causes the radial centroid of the flame to move azimuthally at a rate equal to the subharmonic frequency. The asymmetry introduced by the off-axis advection of the flame in the heat release rate spatial distribution was shown to yield acoustic resonance at the subharmonic time scale in

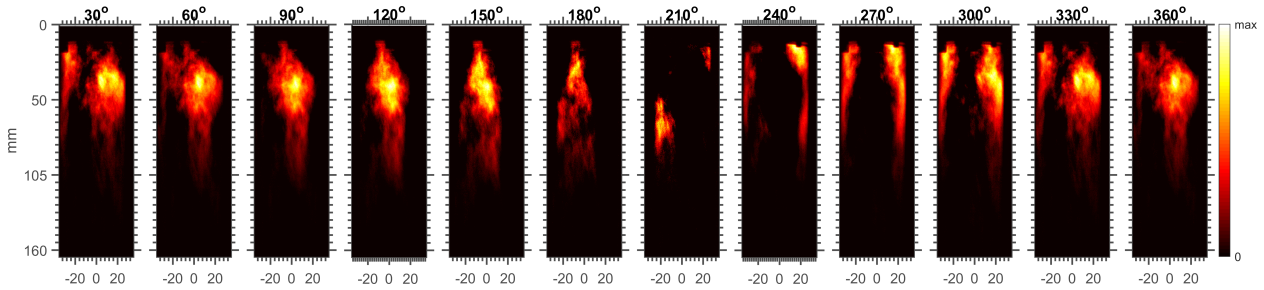


Fig. 10 DMD phase shifted reconstruction of the flame structure in respect to the Dynamic Mode identified at the subharmonic frequency. The periodicity of the phenomenon instead of the fundamental dynamic pressure of oscillations is the subharmonic frequency, hence the time distance between successive phase angles is 1.05 ms**. The contours show the intensity of the spatial distribution of CH^* chemiluminescence.**

[31], hence the subharmonic signature in the dynamic pressure spectra.

The demonstration of the PVC and flame interaction in the Case 2 flame is attempted in Fig. 10. Description of the contribution of the subharmonic flame structures is pursued by applying Dynamic Mode Decomposition (DMD) on high speed flame images. All frequencies are filtered except for the one related to the subharmonic frequency of instability, in order to isolate the coherent structure associated explicitly with the timescale of interest. Details of the DMD algorithm can be found in [37] and an application on a gas turbine combustor can be found in [38] and in [12]. The results of the reconstruction show an azimuthally convected high heat release rate region. Its intensity is not constant throughout its spinning period but it rather decreases when it traverses towards the wall of the negatively signed radial half of the combustor. The period of this coherent structure is equal to the subharmonic period of instability, hence successive images of flame structures resolve 1.05ms. The azimuthal advection of the high heat release rate area in conjunction with the fluctuating intensity, that introduces resonance at this frequency hints towards the significant contribution of the coherent structure in the establishment of the period doubling bifurcation.

It is of further interest to examine the phase averaged flame structure in respect to the fundamental period of instability. Figure 11 describes the phase averaged flame shapes for Case 1 (top) and Case 2 (bottom). Case 1 features a V-shaped flame, whose main anchoring location appears to be mainly the region between the wall boundary layers and the outer shear layers of the recirculation zone. On increasing equivalence ratio, in Case 2 the flame assumes an M-shape, meaning it is able to anchor both on the previous anchoring location and along the inner shear layers of the combustor. The anchoring locations of the flame have been shown in [39], in the current experimental configuration, and in [40] to be largely dependent on the flow imposed strain rate that the flame experiences. In the latter work, the authors show that a V- shaped flame bifurcates to an M-shape on increasing the equivalence ratio, hence increasing the tolerance of the flame to increased flow imposed strain. Moreover, the discussion and the results up to this point have shown that there exists evidence that the period doubling bifurcation comes about if the flame is able to anchor on the shear layers of the recirculation zone. When it achieves concrete anchoring in these regions of the topology of the flow field, and does not extinguish due to the high strain rates at the inlet of the combustor the flame is bound to be affected by the helical shear layer instabilities. Enhanced mixture extinction strain rates are achieved by increasing the equivalence ratio. In contrast, if the Reynolds number and equivalence ratio are kept constant, a potential reduction of the mixture extinction strain rate shall deter the flame from anchoring in the shear layers and eventually suppress the signature of the subharmonic on the dynamic pressure and heat release rate spectra. Those considerations motivated the experiments whose results are presented in the following section. The fuel's propane molar fraction is decreased by adding nitrogen to act as an inert diluent. The mixture extinction strain rate is decreased, while the effect on the adiabatic temperature of combustion T_{ad} is expected to be decreasing but limited, as the change in the total molar fraction of nitrogen in the oxidizer and fuel premixture is limited as well.

IV. Effect of Nitrogen Dilution on the Dynamic State

Figure 12 shows the effects of nitrogen dilution on the dynamic state of the combustor as well as on the mixture characteristics as a function of the molar fraction of the inert diluent in the fuel mixture. Figure 12a left (red circles)

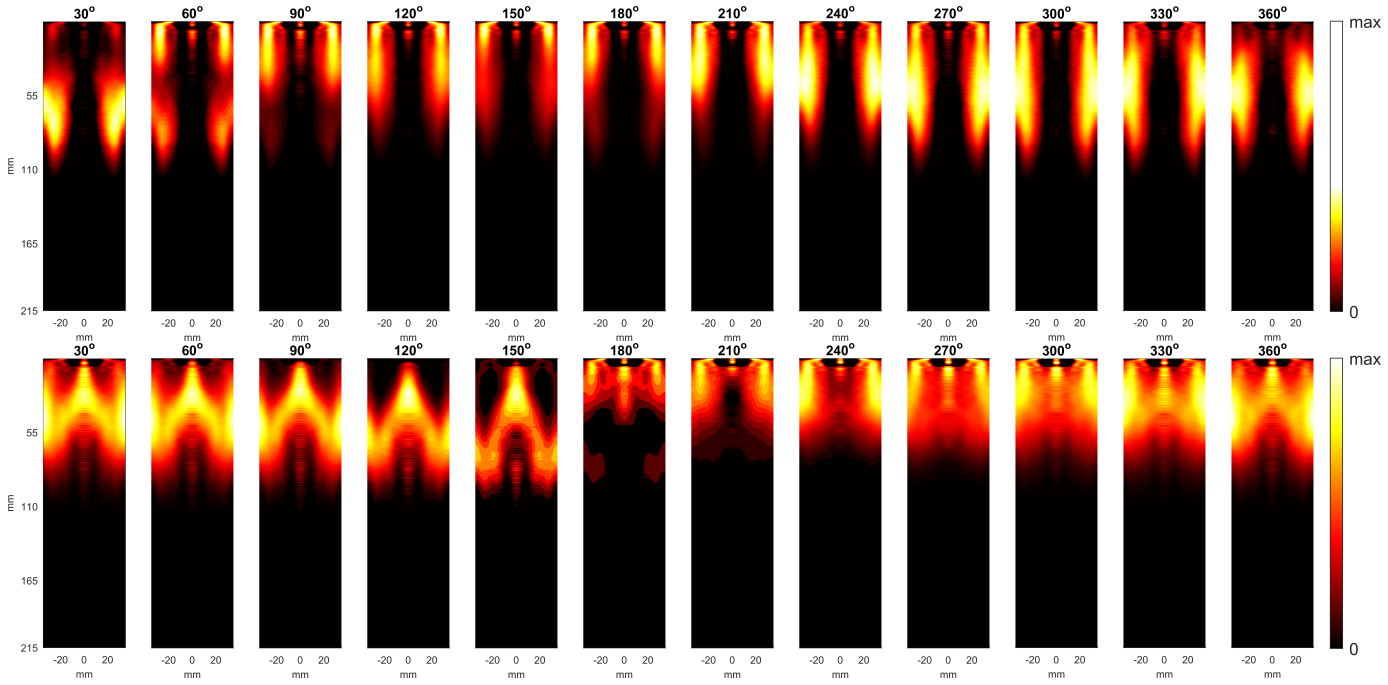


Fig. 11 Top: Phase averaged CH* intensity distribution of the ϕ=0.55 flame, Period-1 limit cycle flame. The flame showcases a V-shape. Bottom: Phase resolved CH* intensity distribution of the ϕ=0.60, Period-2 flame. The flame showcases an M-shape. Phase averaging is pursued in respect the fundamental frequency of oscillations, with maximum dynamic pressure occurring at phase angle 360^0 and minimum dynamic pressure occurring at phase angle 180^o. The time interval between successive phase angles is 0.525 ms.

and right axis (green crosses) show the dynamic pressure fundamental amplitude and frequency respectively. One observes a consistently decreasing trend for both quantities. The most significant decrease is the one observed for the amplitude of dynamic pressure since the ordinate is described in a logarithmic dBa scale. Figure 12b shows the trends for the subharmonic dynamic pressure amplitude and frequency. The frequency of the subharmonic oscillations follows a consistently decreasing trend. Interestingly, even though the respective subharmonic amplitude remains fairly constant for intermediate dilution values, the maximum dilution fraction comes about with an abrupt reduction of the subharmonic amplitude. The value it attains at 50% dilution rate is barely distinguishable from the background amplitude of the dynamic pressure fluctuations. Furthermore, Fig. 12c shows the amplitude of the fundamental frequency of the upstream duct standing wave velocity oscillations at an axial section just upstream the inlet of the swirler. The impinging on the swirler velocity fluctuations follow a consistently decreasing trend. The fluctuations have been inferred by the two microphone method [15], which has been applied in various same purpose experimental works such as [26, 41]. Finally, Fig. 12d left (red circles) and right (green crosses) axis describe the decreasing trend on increasing dilution fuel fractions of the Lower Wobbe Index (LWI) and the extinction strain rate k_{ext} respectively. The LWI is defined as the lower heating value of the fuel gas divided by the square root of its specific gravity. Mixture properties have been calculated through the software Cantera [22] using the GRI-3.0 reaction mechanism. The LWI is decreased by a maximum of 10% in respect to the 0% molar fraction value. The effect of dilution on the mixture extinction however is more significant as a 30% reduction is introduced for 50% diluent molar fraction.

The described set of sub-figures indicates that a reduction in the adiabatic flame temperature equal to 50% of the flame temperature difference between Cases 1 and 2, as registered in Table 1 affects the fundamental dynamic properties of the limit cycle. However, the effect of the diluent introduction is not limited solely to a reduction of the adiabatic flame temperature. According to [9] and [42], fuel dilution adjusts the convective time delay τ, because the flame anchoring locations are adjusted. The effect on the flame shape in the current geometry is examined in the following section. Nevertheless, the phase difference between the dynamic pressure and heat release rate is indicative of the time delay τ, as this quantity has been shown to dictate the thermoacoustic coupling strength [43], [44]. Figure 13 shows

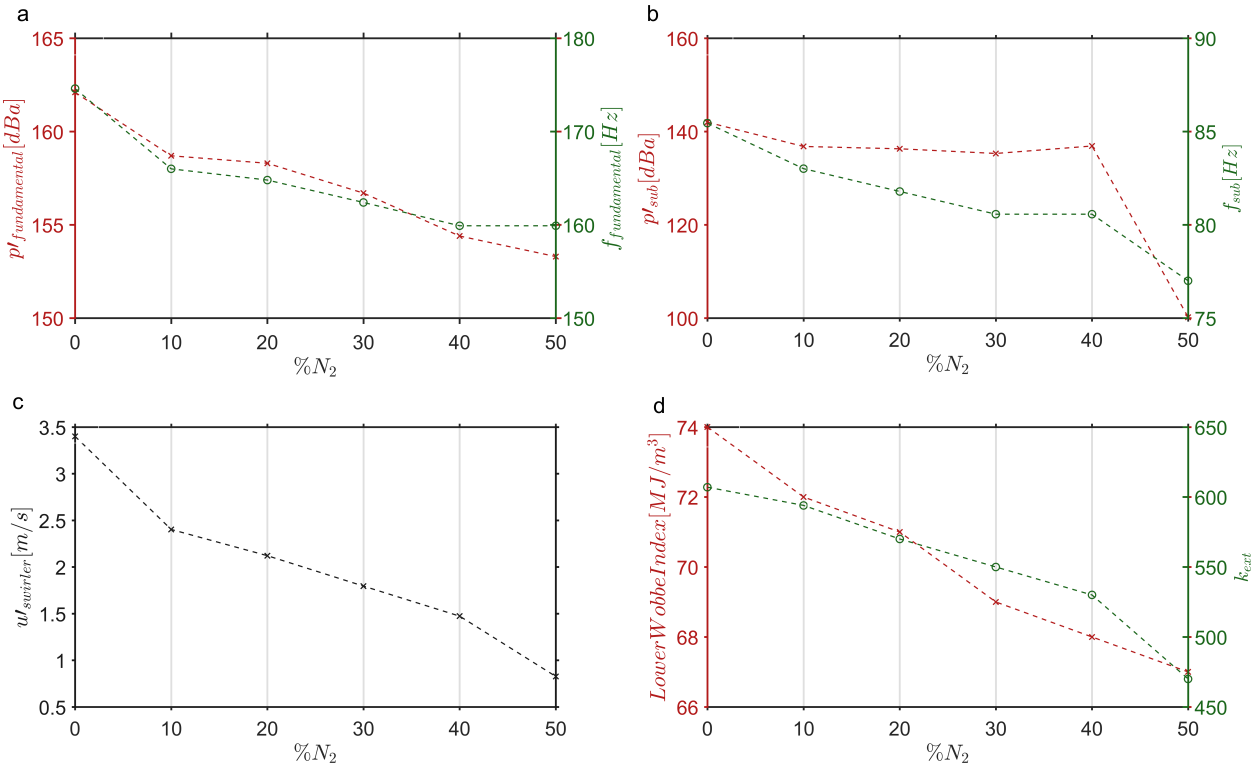


Fig. 12 The abscissa of the subfigures is the molar fraction of the fuel N_2-dilution. a) Dynamic pressure fundamental amplitude (left axis-red crosses) and dynamic pressure fundamental frequency (right axis green circles). b) Dynamic pressure subharmonic amplitude (left axis-red crosses) and dynamic pressure subharmonic frequency (right axis green circles). c) Amplitude of the fundamental frequency of the velocity of the established standing wave at an axial section $0.630\,\mathrm{m}$ downstream the sonic nozzle, upstream the inlet of the swirler. d) The Lower Wobbe Index and the extinction strain rate calculated *via* Cantera.

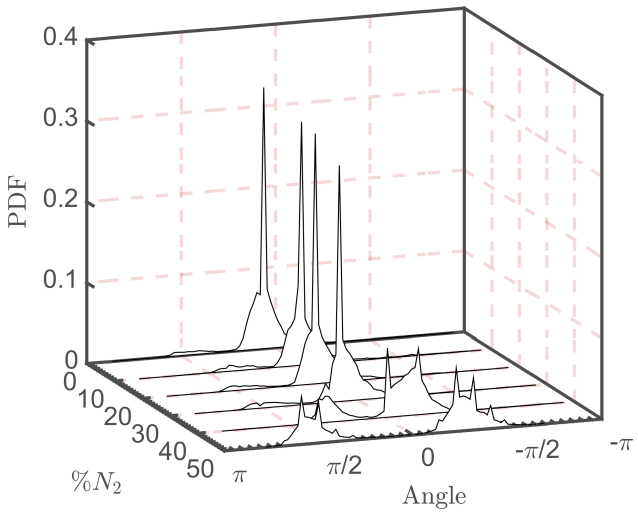


Fig. 13 Phase difference probability distribution between the dynamic pressure and CH^* signals as a function of the molar fraction of the fuel N_2-dilution.

histograms of the probability distribution of the phase difference between dynamic pressure and heat release rate, with the inert molar fraction in the fuel as a parameter. It is interesting to note that up to a dilution fraction of 30% the angle of most probable coupling remains close to zero radians, with a slightly decreasing probability for cases with higher diluent molar fractions. The change of the coupling angle probability distribution is significant for nitrogen molar fractions 40% and 50%. The former case, showcases distinctively decreased probability of coupling at zero radians and an additional equally high probability at $pi/4$. In the latter case, the coupling histogram features increased contribution in an out of phase range $[\pi/2,\pi]$, while the in-range part of the histogram, namely the range $[0,\pi/2]$ features high probability coupling values at a range away from zero radians. Hence, nitrogen addition adjusts the flame anchoring locations in such a way that the coupling strength of dynamic pressure pressure and heat release rate decreases. Having described the effects of nitrogen dilution on the dynamic state of operation of the combustor, the next section considers the respective effects on the flow and flame shape.

V. Effect of Nitrogen Dilution on Flame and Flow Shape

Figure 14 shows the effect of increasing nitrogen dilution on the mean flow calculated from instantaneous flowfields under limit cycle combustor operation. Even though the mean flow in the current geometry is not representative of the coherent component during limit cycle oscillations, this set of subfigures assists in identifying the effect of nitrogen dilution on the extent of the recirculation zone and on the swirl number fluctuations. Based on Fig.12c on increasing the molar fraction of the diluent, the amplitude of the velocity fluctuations decreases. In [36], the authors show that swirl number fluctuations can be introduced by a mode conversion process, wherein azimuthal disturbances, induced by axial wave-swirler interference, convect downstream at the bulk velocity. It is showed that this phase difference between axial and azimuthal disturbances causes the swirl number to fluctuate, according to equation 2, where S is the swirl number, u and v denote the axial and azimuthal components of velocity respectively.

$$\frac{S}{\bar{S}} = \left[1 + \frac{v\prime}{\bar{v}} - \frac{u\prime}{\bar{u}}\right] \tag{2}$$

According to [45], the extent of the vortex breakdown induced recirculation zone increases on increasing swirl number and vice versa. Hence, we can conclude that on increasing amplitude of incident velocity oscillations, swirl number fluctuations are induced, which eventually introduce oscillations in the extent of the recirculation zone. These remarks aid in justifying the increasing extent of the recirculation zone on increasing dilution. The swirl number fluctuations decrease since the effective amplitude of azimuthal disturbances is suppressed, hence the fluctuation of the axial extent of the recirculation zone is limited. This effect is further studied in respect to the limit cycle phase averaged flow field structure in Fig. 16-18.

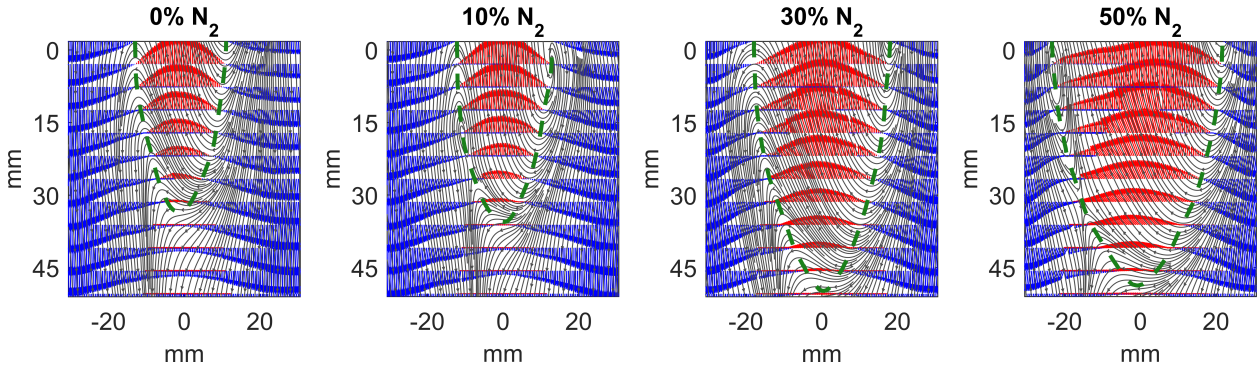


Fig. 14 Mean flow field structure in respect to the fuel diluent N_2 molar fraction. Streamlines are superimposed on red and blue coloured vectors that mark negative and positive axial velocity regions respectively. The green dashed lines indicate the extent of the recirculation region.

The effects of inert dilution on the flame shape on increasing diluent content are shown in Fig. 15. Results are presented from 30% up to 50% diluent molar fraction cases. The case with 30% nitrogen dilution demonstrated Period-2 oscillations, featuring an M-shaped flame, similar to the one presented in Fig. 11(bottom). However, the intensity in the inner shear layers anchoring regions is reduced in comparison to the 0% case. On further increasing the molar fraction of the diluent, the flame recedes from the inner shear layers of the recirculation zone and it bifurcates back to a V-shape similar to the shape of the flame with 0% dilution and $\phi = 0.55$, which demonstrated period-1 limit cycle oscillations. These observations, along with the ones presented in section III, indicate that the period doubling bifurcation is directly linked with the ability of the flame to sustain anchoring on the high strain regions at the combustor inlet, and effectively on the inner shear layers.

The effect of inert dilution on the coherent structure of the flowfield over a period of thermoacoustic instability is examined next. The flowfield structure of the case with 50% diluent molar fraction is presented in pairs Fig. 16 and Fig. 17, upon which the same phase averaged streamlines are superimposed on contours of axial velocity and flow imposed strain rate respectively. The same contours corresponding to the flowfield phase averaged coherent structure of the 0% case are presented Fig. 18 and 19. The comparison of the axial velocities of the two cases reveals that as concluded from Fig. 14 the oscillation of the extent of the recirculation zone is enhanced for the 0% in comparison with the 50%. High velocity regions are induced due to reaction-induced flow dilatation. Comparing the two cases, it is observed that the 0% case features significantly higher velocities, since the laminar flame speed is greater given the mixture properties. The enhanced dilatation rates lead to increased velocity gradients and flow imposed strain rates as well. For comparison purposes between the two cases the strain rate contours are normalized against the ratio of the bulk velocity U_{bulk} over the combustor diameter D. Nevertheless, replotting the strain rate contours normalized over the extinction strain rates of the mixtures in Fig. 20 aids in revealing the mechanism that dictates whether the flame sustains anchoring on the inner shear layers. The strain rate the flame is exposed to by the flow structure is calculated based on the approach suggested in [40]. Significantly, higher strain rate ratios are observed for the 50% dilution case, meaning that this flame is more susceptible to extinction than the 0% dilution case, thereby it would not be able to penetrate through the high flow imposed strain rate regions developed from phase angles 240^o up to 360^o (see Fig. 20(top)). Considering that the Lewis number of the mixture is greater than unity for propane, increasing the strain the flame is exposed to, leads to reduced heat release rate values [24]. It is hence inferred that the molar fraction of inert diluents in the fuel can greatly affect the anchoring location on the flowfield and thereby the dynamic state that the combustor operates in.

VI. Conclusions

The current paper examined the effects of the existence of inert diluents in the fuel on the dynamic state of a turbulent swirl-stabilized model combustor. The addition of inert diluents was limited to 10% Wobbe index adjustment in respect to the undiluted fuel. Optical experiments were carried out on a model gas turbine combustor that included high speed time resolving Particle Image Velocimetry on a radial-axial section and high speed CH^* chemiluminescent imaging

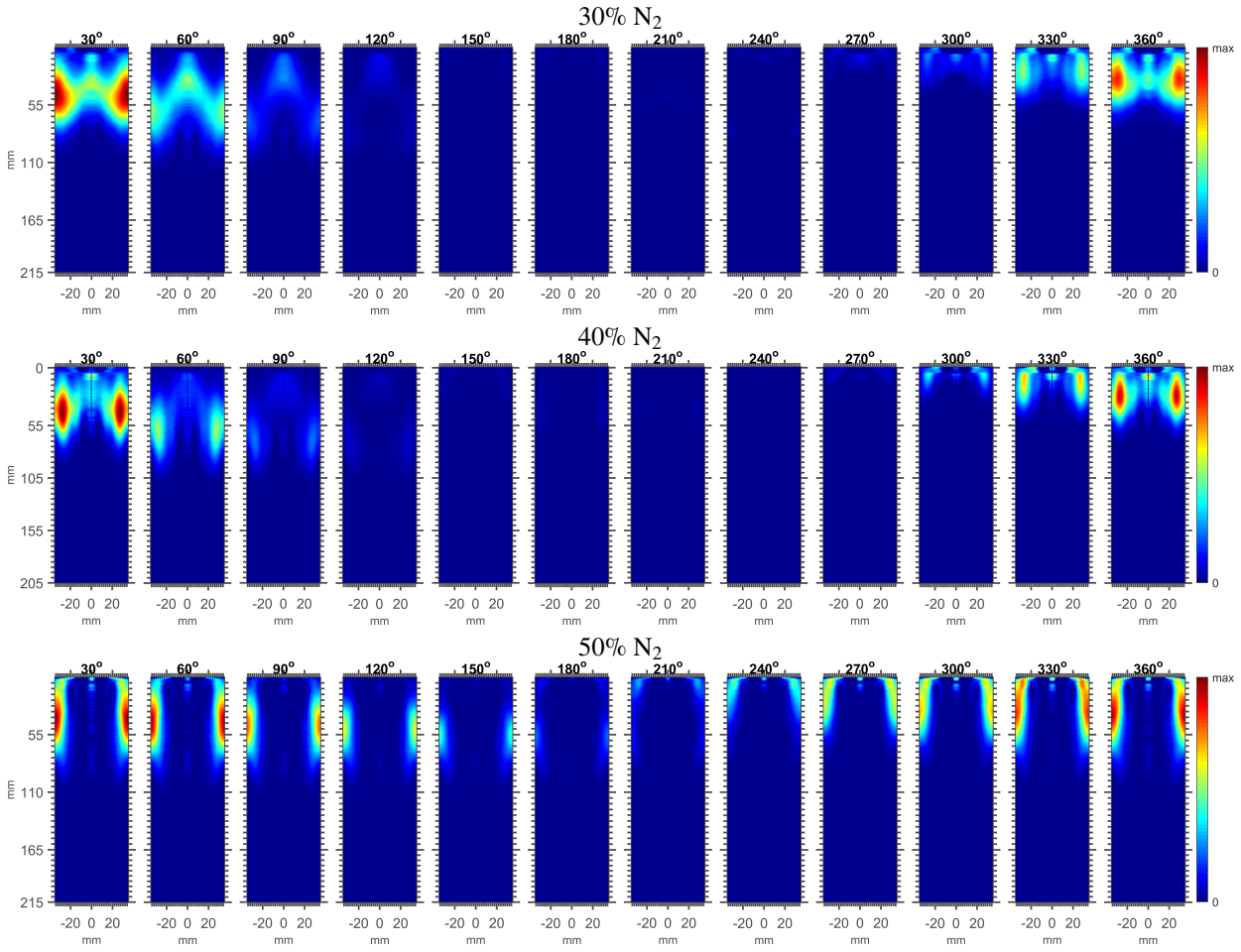


Fig. 15 Phase averaged flame shape identified via CH^* high speed chemiluminescent intensity measurements. Nitrogen dilution was increased while the equivalence ratio was kept constant. On increasing nitrogen dilution the flame bifurcated from an M- to a V-shape. The time distance between successive phase angles is 0.525 ms**.**

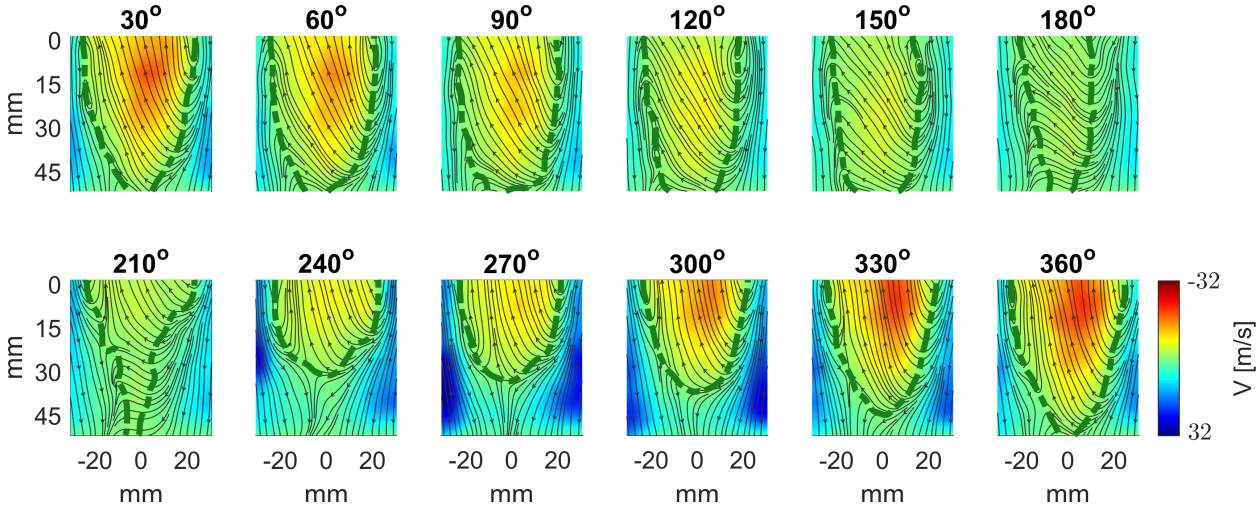


Fig. 16 50% N_2: Phase averaged streamlines superimposed on contours of axial velocity V.

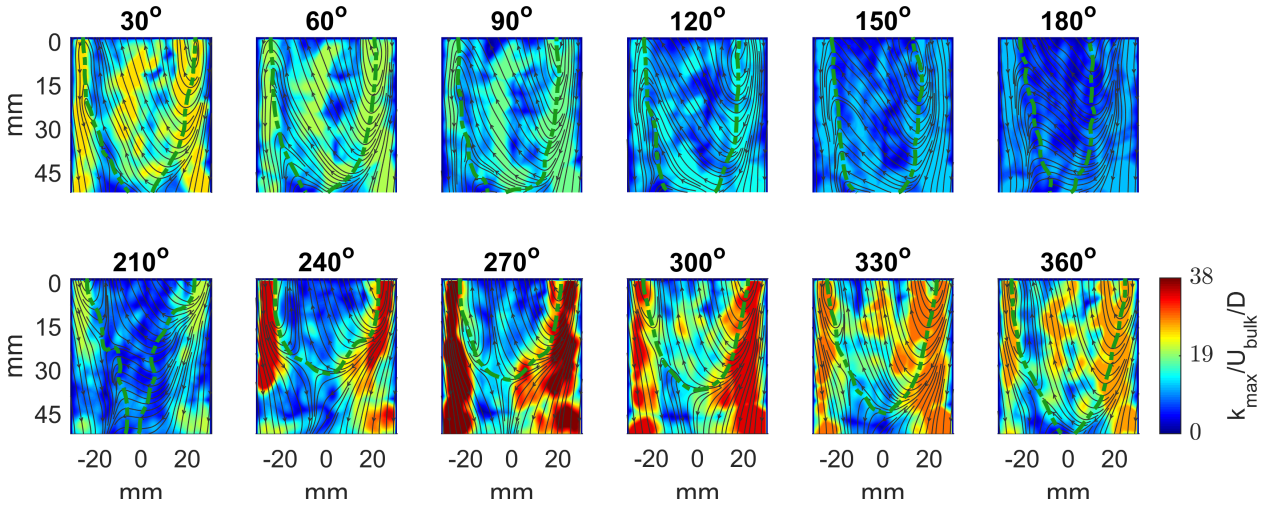


Fig. 17 50% N_2: Phase averaged streamlines superimposed on contours of normalized flow imposed strain rate k_{max}. The normalization parameter is the bulk velocity in the combustor U_{bulk} and the combustor diameter D.

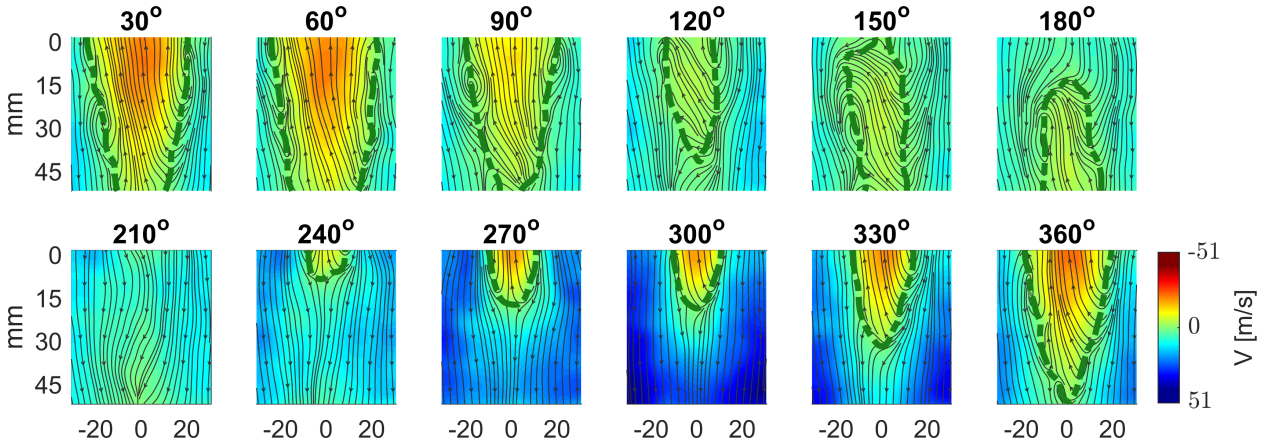


Fig. 18 0% N_2: Phase averaged streamlines superimposed on contours of axial velocity V.

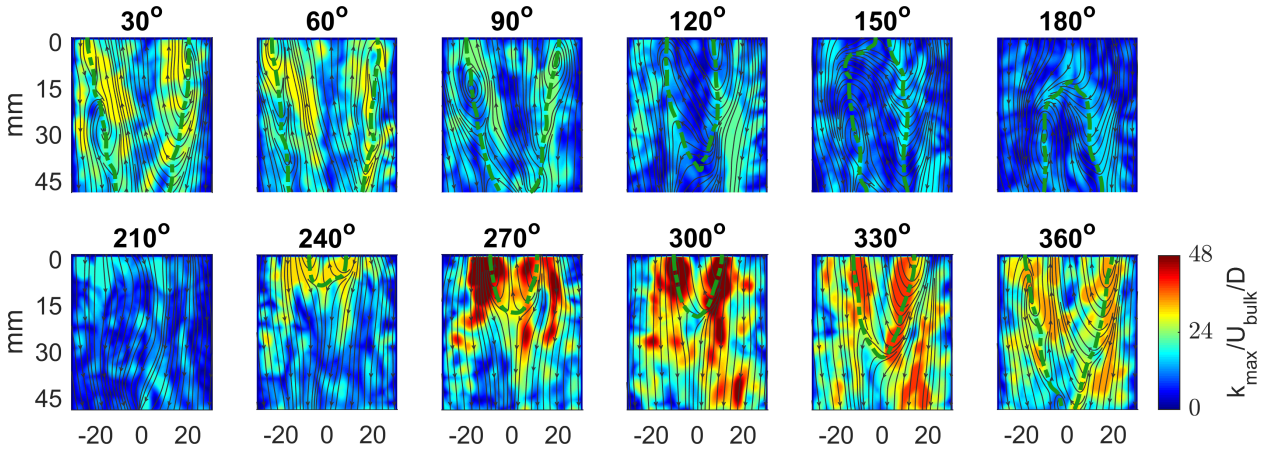


Fig. 19 0% N_2: Phase averaged streamlines superimposed on contours of normalized flow imposed strain rate k_{max}. The normalization parameter is the bulk velocity in the combustor U_{bulk} and the combustor diameter D.

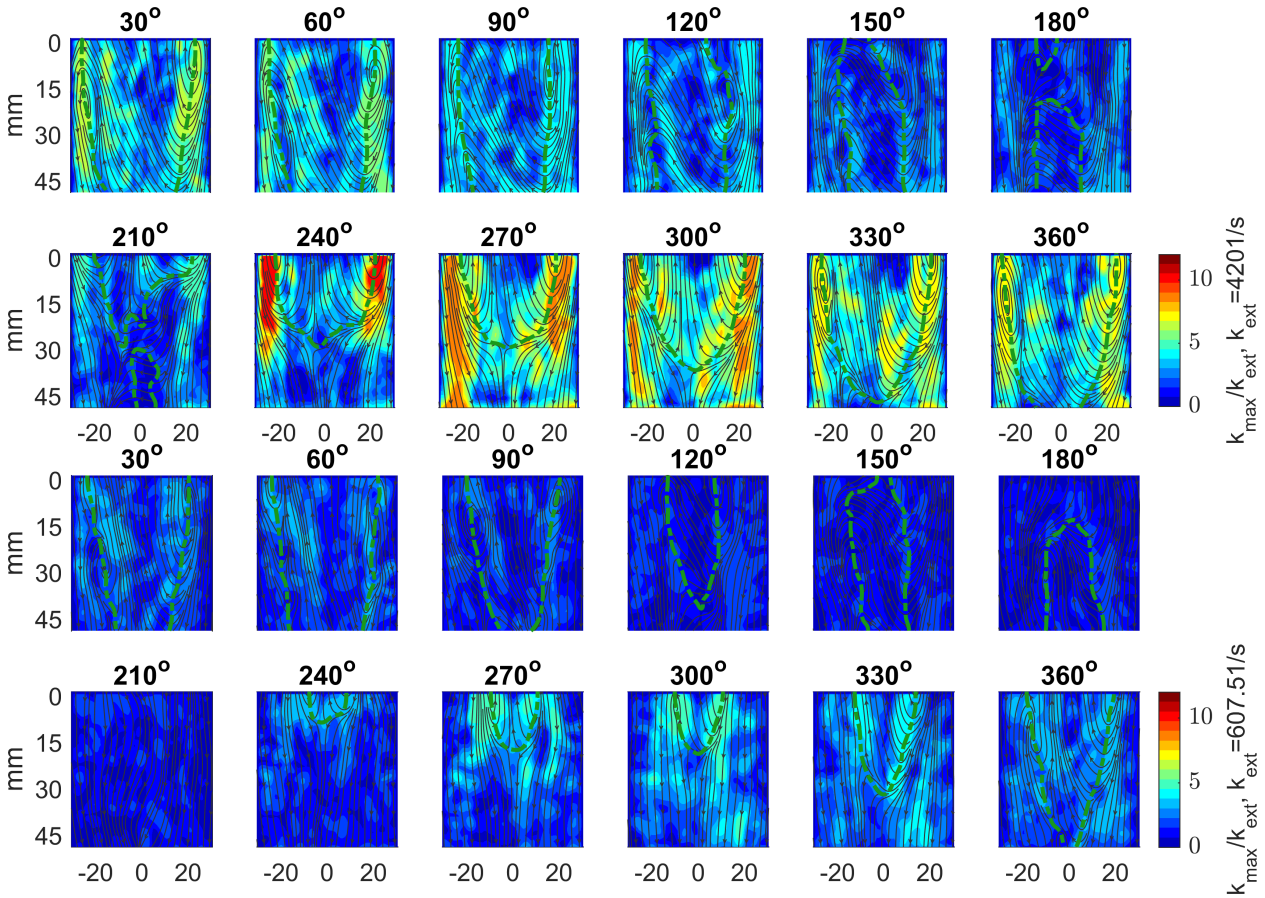


Fig. 20 Same phase averaged flowfield streamlines as the ones presented in Fig. 17 and 19 but the contours are normalized over the extinction strain rate of the mixture. The scales of the colour bars are the same in both figures to aid comparison between the two cases.

on the same plane. The paper focused on the operational conditions and the fuel properties under which the period doubling bifurcation came about. It was initially shown that, on increasing the equivalence ratio from 0.55 to 0.60 for undiluted propane-air premixture, the dynamics in addition to the fundamental acoustic timescale were dictated by a subharmonic, aerodynamic in nature timescale. The 0.60 equivalence ratio propane mixture was then diluted with nitrogen. Conditions of up to 50% nitrogen molar fractions in the fuel were examined to challenge the research hypothesis that the extinction strain rate of the mixture dictates the anchoring locations of the flame and effectively the dynamic state the combustor operates in. The main findings are summarized in the following points:

- For undiluted propane combustion the emergence of the subharmonic on increasing the equivalence ratio came about with a flame shape bifurcation from a V- to an M-shaped flame. The flame further to anchoring between the outer shear layers and the boundary walls of the combustor in a V-shape configuration, expanded on the inner shear layers, assuming an M-shape.
- Dynamic Mode Decomposition was applied on the Period-2 flame to explicitly depict the coherent flame structure associated with the subharmonic frequency. A high heat release rate structure was advected azimuthally at the subharmonic timescale. Importantly, the structure demonstrated intensity asymmetries during its azimuthal convection as quenching was observed when it traversed to the opposite side of the centroid location of highest intensity. According to the relevant literature, such asymmetries induce resonance at the subharmonic mode and they are a characteristic aspect of swirl stabilized combustors under the influence of the Precessing Vortex Core.
- Nitrogen dilution of the fuel resulted in gradually decreasing coupling strength between the dynamic pressure and global heat release rate signals. This resulted in a reduction in both the amplitude and the frequency of the dynamic pressure fundamental mode. Interestingly, the amplitude of the subharmonic mode showcased a sharp decrease in the dynamic pressure spectra only after the flame receded from the inner shear layers of the flowfield.

- The amplitude of the fundamental velocity oscillations of the standing wave established upstream the swirler and downstream the sonic nozzle was reduced on increased nitrogen dilution molar fractions. This resulted in mitigated swirl number fluctuations, hence oscillations of the axial extension of the recirculation zone were suppressed.
- On increasing diluent molar fraction under an equivalence ratio equal to 0.60, the flame bifurcated back to a V-shape similar to the flame configuration for an equivalence ratio of 0.55. Meanwhile, the Period-2 limit cycle was also suppressed into a Period-1 limit cycle.
- A comparison of the coherent structure of the flowfield during the limit cycle was carried out between the undiluted 0.60 equivalence ratio flame and the flame with 50% molar fraction at the same equivalence ratio. It was found that the former case features higher velocity values, hence the flame experienced higher strain rates. This was attributed to the enhanced laminar flame speeds of the undiluted propane mixture, which inferred increased dilatation rates.
- Even though, in absolute terms the non-diluted flame experienced higher strain rates, normalizing the flow imposed strain rate over the extinction strain rate showed that the diluted flame experienced higher straining than its quenching threshold. This is the mechanism responsible for the flame's recession away from the inner shear layers. Thus, one can explain the shape of the flame for the 0.55 equivalence ratio flame and for the high dilution molar fraction cases.

Acknowledgements

The authors would like to acknowledge support from the Engineering and Physical Sciences Research Council (EPSRC) through grants EP/K21095/1 and EP/M0153001/1. The authors are also grateful to SIEMENS UK Industrial Turbomachinery Ltd. for their support.

References

[1] Correa, S. M., "A Review of NOx Formation Under Gas-Turbine Combustion Conditions," *Combustion Science and Technology*, Vol. 87, No. 1-6, 1993, pp. 329–362. doi:10.1080/00102209208947221.

[2] Casleton, K. H., Breault, R. W., and Richards, G. A., "System issues and tradeoffs associated with syngas production and combustion," *Combustion Science and Technology*, Vol. 180, No. 6, 2008, pp. 1013–1052.

[3] Lieuwen, T. C., *Unsteady combustor physics*, Cambridge University Press, 2012.

[4] Dowling, A. P., "Nonlinear self-excited oscillations of a ducted flame," *Journal of Fluid Mechanics*, Vol. 346, 1997, pp. 271–290. doi:10.1017/S0022112097006484.

[5] Taamallah, S., Vogiatzaki, K., Alzahrani, F., Mokheimer, E., Habib, M., and Ghoniem, A., "Fuel flexibility, stability and emissions in premixed hydrogen-rich gas turbine combustion: Technology, fundamentals, and numerical simulations (vol 154, pg 1020, 2015)," *Applied Energy*, Vol. 219, 2018, pp. 426–426.

[6] Janus, M. C., Richards, G. A., Yip, M. J., and Robey, E. H., "Effects of ambient conditions and fuel composition on combustion stability," *ASME 1997 International Gas Turbine and Aeroengine Congress and Exhibition*, American Society of Mechanical Engineers, 1997, pp. V002T06A035–V002T06A035.

[7] Lieuwen, T., McDonell, V., Petersen, E., and Santavicca, D., "Fuel flexibility influences on premixed combustor blowout, flashback, autoignition, and stability," *Journal of engineering for gas turbines and power*, Vol. 130, No. 1, 2008, p. 011506.

[8] Figura, L., Lee, J. G., Quay, B. D., and Santavicca, D. A., "The effects of fuel composition on flame structure and combustion dynamics in a lean premixed combustor," *ASME Turbo Expo 2007: Power for Land, Sea, and Air*, American Society of Mechanical Engineers, 2007, pp. 181–187.

[9] Ferguson, D., and Ranalli, J., "Characterization of Instabilities in a Low-Swirl Injector with Exhaust Gas Recirculation," *AIAA Journal*, 2011, pp. 1–9. doi:10.2514/6.2011-517.

[10] Shanbhogue, S. J., Sanusi, Y. S., Taamallah, S., Habib, M. A., Mokheimer, E. M. A., and Ghoniem, A. F., "Erratum to " Flame macrostructures , combustion instability and extinction strain scaling in swirl-stabilized premixed CH 4 / H 2,"

Combustion and Flame, Vol. 167, 2016, p. 497. doi:10.1016/j.combustflame.2016.02.015, URL http://dx.doi.org/10.1016/j.combustflame.2016.02.015.

[11] Taamallah, S., Shanbhogue, S. J., and Ghoniem, A. F., "Turbulent flame stabilization modes in premixed swirl combustion: Physical mechanism and Karlovitz number-based criterion," *Combustion and Flame*, Vol. 166, 2016, pp. 19–33. doi:10.1016/j.combustflame.2015.12.007, URL http://dx.doi.org/10.1016/j.combustflame.2015.12.007.

[12] Noh, D., Karlis, E., Navarro-Martinez, S., Hardalupas, Y., Taylor, A., Fredrich, D., and Jones, W., "Azimuthally-driven subharmonic thermoacoustic instabilities in a swirl-stabilised combustor," *Proceedings of the Combustion Institute*, 2018.

[13] Bayley, A. E., Hardalupas, Y., and Taylor, A. M., "Local curvature measurements of a lean, partially premixed swirl-stabilised flame," *Experiments in Fluids*, Vol. 52, No. 4, 2012, pp. 963–983. doi:10.1007/s00348-011-1181-4, URL http://link.springer.com/10.1007/s00348-011-1181-4.

[14] Panoutsos, C. S., Hardalupas, Y., and Taylor, A. M. K. P., "Effect of Preheating on the local Equivalence Ratio at a," *41st Aerospace Sciences Meeting and Exhibit, AIAA 2008-0960*, , No. January, 2008, pp. 1–13.

[15] Åbom, M., and Bodén, H., "Error analysis of two-microphone measurements in ducts with flow," *The Journal of the Acoustical Society of America*, Vol. 83, No. 6, 1988, pp. 2429–2438. doi:10.1121/1.396322, URL http://asa.scitation.org/doi/10.1121/1.396322.

[16] Lieuwen, Timothy, C., and Yang, V., "Combustion Instabilities in Gas Turbine Engines: Operational Experience, Fundamental Mechanisms, and Modeling," Vol. 210, 2005, pp. 8–9. URL http://www.gbv.de/dms/goettingen/502348356.pdf.

[17] Lilley, D. G., "Swirl Flows in Combustion: A Review," *AIAA Journal*, Vol. 15, No. 8, 1977, pp. 1063–1078. doi:10.2514/3.60756, URL http://arc.aiaa.org/doi/10.2514/3.60756.

[18] Orain, M., and Hardalupas, Y., "Influence du combustible sur la mesure de richesse par chimiluminescence dans les flammes prémélangées," *Comptes Rendus - Mecanique*, Vol. 338, No. 5, 2010, pp. 241–254. doi:10.1016/j.crme.2010.05.002, URL http://dx.doi.org/10.1016/j.crme.2010.05.002.

[19] Karlis, E., Hardalupas, Y., and Taylor, A. M., "Experimental characterization of intermittency of thermoacoustic instability in a swirl stabilized combustor. 1," *European Combustion Meeting (ECM)*, 2017, pp. 18–21.

[20] Bayley, A. E., "Turbulent Flow Structure and Flame Characterisation of Lean Premixed Swirling Combustion," Ph.D. thesis, 2014.

[21] Peters, N., *Turbulent combustion*, IOP Publishing, 2001.

[22] Goodwin, D., "Cantera," https://code.google.com/archive/p/cantera/, 2003-2018.

[23] Smith, G. P., Golden, D. M., Frenklach, M., Moriarty, N. W., Eiteneer, B., Goldenberg, M., Bowman, C. T., Hanson, R. K., Song, S., Gardiner Jr, W., et al., "GRI-Mech 3.0, 1999," *URL http://www. me. berkeley. edu/gri_mech*, 2011.

[24] Lipatnikov, A., *Fundamentals of premixed turbulent combustion*, CRC Press, 2012.

[25] Takens, F., "Detecting Strange Attractors in Turbulence," *Lecture Notes in Mathematics1*, Vol. 898, 1981, pp. 336–381. doi:10.1007/bfb0091924.

[26] Kim, K., Lee, J., Quay, B., and Santavicca, D. A., "Spatially distributed flame transfer functions for predicting combustion dynamics in lean premixed gas turbine combustors," *Combustion and Flame*, Vol. 157, No. 9, 2010, pp. 1718–1730. doi:10.1016/j.combustflame.2010.04.016, URL http://www.sciencedirect.com/science/article/pii/S0010218010001203{%}5Cnhttp://linkinghub.elsevier.com/retrieve/pii/S0010218010001203.

[27] Dowling, A. P., Stow, S. R. S., and Kingdom, U., "Acoustic Analysis of Gas Turbine Combustors," *Journal of Propulsion and Power*, Vol. 19, No. 5, 2003, pp. 751–764. doi:10.2514/2.6192, URL http://arc.aiaa.org/doi/pdf/10.2514/2.6192.

[28] Strutt, J. W., *The explanation of certain acoustical phenomena*, 1948. doi:10.1017/CBO9780511491757.014.

[29] Boxx, I., Stöhr, M., Carter, C., and Meier, W., "Temporally resolved planar measurements of transient phenomena in a partially pre-mixed swirl flame in a gas turbine model combustor," *Combustion and Flame*, Vol. 157, No. 8, 2010, pp. 1510–1525. doi:10.1016/j.combustflame.2009.12.015, URL http://dx.doi.org/10.1016/j.combustflame.2009.12.015.

[30] Terhaar, S., Oberleithner, K., and Paschereit, C. O., "Impact of Steam-Dilution on the Flame Shape and Coherent Structures in Swirl-Stabilized Combustors," *Combustion Science and Technology*, Vol. 186, No. 7, 2014, pp. 889–911. doi:10.1080/00102202.2014.890597, URL http://www.tandfonline.com/doi/abs/10.1080/00102202.2014.890597.

[31] Moeck, J. P., Bourgouin, J. F., Durox, D., Schuller, T., and Candel, S., "Nonlinear interaction between a precessing vortex core and acoustic oscillations in a turbulent swirling flame," *Combustion and Flame*, Vol. 159, No. 8, 2012, pp. 2650–2668. doi:10.1016/j.combustflame.2012.04.002, URL http://dx.doi.org/10.1016/j.combustflame.2012.04.002.

[32] Oberleithner, K., Stöhr, M., Im, S. H., Arndt, C. M., and Steinberg, A. M., "Formation and flame-induced suppression of the precessing vortex core in a swirl combustor: Experiments and linear stability analysis," *Combustion and Flame*, Vol. 162, No. 8, 2015, pp. 3100–3114. doi:10.1016/j.combustflame.2015.02.015, URL http://dx.doi.org/10.1016/j.combustflame.2015.02.015.

[33] Gallaire, F., and Chomaz, J. M., "Instability mechanisms in swirling flows," *Physics of Fluids*, Vol. 15, No. 9, 2003, pp. 2622–2639. doi:10.1063/1.1589011.

[34] Loiseleux, T., and Chomaz, J.-m., "Breaking of rotational symmetry in a swirling jet experiment," *Physics of Fluids*, Vol. 15, No. 2003, 2004, pp. 511–522. doi:10.1063/1.1533068.

[35] Juniper, M. P., Tammisola, O., and Lundell, F., "The local and global stability of confined planar wakes at intermediate Reynolds number," *Journal of Fluid Mechanics*, Vol. 686, 2011, pp. 218–238. doi:10.1017/jfm.2011.324.

[36] Palies, P., Durox, D., Schuller, T., and Candel, S., "The combined dynamics of swirler and turbulent premixed swirling flames," *Combustion and Flame*, Vol. 157, No. 9, 2010, pp. 1698–1717. doi:10.1016/j.combustflame.2010.02.011, URL http://dx.doi.org/10.1016/j.combustflame.2010.02.011.

[37] Schmid, P. J., "Dynamic mode decomposition of numerical and experimental data," *Journal of Fluid Mechanics*, Vol. 656, 2010, pp. 5–28. doi:10.1017/S0022112010001217.

[38] Labry, Z. A., Shanbhogue, S. J., Speth, R. L., and Ghoniem, A. F., "Flow structures in a lean-premixed swirl-stabilized combustor with microjet air injection," *Proceedings of the Combustion Institute*, Vol. 33, No. 1, 2011, pp. 1575–1581. doi:10.1016/j.proci.2010.06.092, URL http://dx.doi.org/10.1016/j.proci.2010.06.092.

[39] Panoutsos, C. S., Hardalupas, Y., and Taylor, a. M. K. P., "Numerical evaluation of equivalence ratio measurement using OH* and CH* chemiluminescence in premixed and non-premixed methane-air flames," *Combustion and Flame*, Vol. 156, No. 2, 2009, pp. 273–291. doi:10.1016/j.combustflame.2008.11.008, URL http://dx.doi.org/10.1016/j.combustflame.2008.11.008.

[40] Shanbhogue, S. J., Sanusi, Y. S., Taamallah, S., Habib, M. A., Mokheimer, E. M. A., and Ghoniem, A. F., "Flame macrostructures, combustion instability and extinction strain scaling in swirl-stabilized premixed CH4/H2 combustion," *Combustion and Flame*, Vol. 163, 2016, pp. 494–507. doi:10.1016/j.combustflame.2015.10.026, URL http://dx.doi.org/10.1016/j.combustflame.2015.10.026http://www.sciencedirect.com/science/article/pii/S001021801500382X.

[41] Ćosić, B., Terhaar, S., Moeck, J. P., and Paschereit, C. O., "Response of a swirl-stabilized flame to simultaneous perturbations in equivalence ratio and velocity at high oscillation amplitudes," *Combustion and Flame*, Vol. 162, No. 4, 2015, pp. 1046–1062. doi:10.1016/j.combustflame.2014.09.025.

[42] Richards, G. A., Straub, D. L., and Robey, E. H., "Passive control of combustion dynamics in stationary gas turbines," *Journal of Propulsion and Power*, Vol. 19, No. 5, 2003, pp. 795–810.

[43] Kim, K. T., "Combustion instability feedback mechanisms in a lean-premixed swirl-stabilized combustor," *Combustion and Flame*, Vol. 171, 2016, pp. 137–151. doi:10.1016/j.combustflame.2016.06.003, URL http://dx.doi.org/10.1016/j.combustflame.2016.06.003.

[44] Lieuwen, T., and Zinn, B. T., "On the experimental determination of combustion process driving in an unstable combustor," *Combustion science and technology*, Vol. 157, No. 1-6, 2000, pp. 111–127. doi:10.1080/00102200008947312.

[45] Beér, J. M., and Chigier, N. A., "Combustion aerodynamics," *New York*, 1972.